Journal of Power Sources 346 (2017) 40–48

Contents lists available at ScienceDirect

Journal of Power Sources

journal homepage: www.elsevier.com/locate/jpowsour

High-performance lithium-ion batteries with 1.5 μm thin copper nanowire foil as a current collector

Hsun-Chen Chu, Hsing-Yu Tuan*

Department of Chemical Engineering, National Tsing Hua University, 101, Section 2, Kuang-Fu Road, Hsinchu, Taiwan 30013, China

HIGHLIGHTS

- Cu NW foil as thin as ~1.5 μm used as a lithium ion battery current collector.
- Graphite-CuNW foil anode exhibits excellent electrochemical performance.
- 3 mAh/cm^2 full cell exhibits 83.6% capacity retention for 600 cycles.
- 700 mA pouch-type battery with graphite-Cu NWs foil anodes is fabricated.

GRAPHICAL ABSTRACT

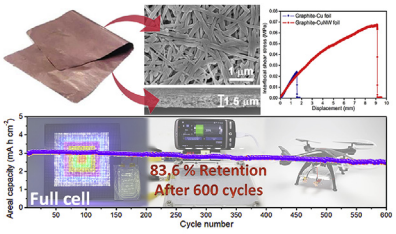

(70 mm x 40 mm, 300 dpi)

ARTICLE INFO

Article history:
Received 5 January 2017
Received in revised form
8 February 2017
Accepted 12 February 2017
Available online 16 February 2017

Keywords:
Copper
Nanowire
Lightweight
Flexible
Large-area
Current collector
Lithium-ion battery

ABSTRACT

Cu Foil, a thin sheet of Cu, is the common anode current collector in commercial lithium ion batteries (LIBs) which accounts for ~ 10 wt% of the total cell weight. However, thickness reduction of LIB-based Cu foils below 6 μm has been limited by the incapability of conventional rolling annealing or electrodeposition process. We here report a new type of Cu foil, so called Cu nanowire foil (CuNW foil), for use as an LIB anode current collector. We fabricate Cu NW foils by rolling press Cu nanowire fabric to reduce the thickness down to ~1.5 μm with an areal weight down to ~1.2 mg cm^{-2} and a density approximately 96% to that of bulk Cu. The rough surface and porous structure of CuNW foil enable better wetting and adhering properties of graphite slurry on foil. In full cell examination, a cell of a areal capacity of 3 mAh cm^{-2} exhibits 83.6% capacity retention for 600 cycles at 0.6 C that meets the standard specification of most commercial LIBs. As a proof-of-concept of demonstration, we fabricate a 700 mA pouch-type battery implemented with graphite-Cu NWs foil anodes to serve as energy supply to operate electronic devices.

1. Introduction

With the advances in technology, the escalation of dependence on cordless power source is greatly considered. Rechargeable lithium-ion batteries (LIBs) have become the most universal energy storage system in modern portable electronics and full/hybrid electric vehicles due to their high energy density, high working voltage, and long cycle life [1–7]. A LIB is an electrochemical system consisting of anode, cathode, separator, current collector, and electrolyte. To accommodate the tendency of the electronic devices that requires lighter weight and longer battery life, a major effort has been made toward increasing energy density associated with a light-weighting design of batteries [8]. The battery energy density could be increased by strategies such as introduction of high capacity electrode materials, increase of the contact area of active materials/electrolyte interface, and reduction of the weight of

* Corresponding author.
E-mail address: hytuan@che.nthu.edu.tw (H.-Y. Tuan).

http://dx.doi.org/10.1016/j.jpowsour.2017.02.041
0378-7753/

battery components [9–18].

Cu foil is the common anode current collector in standard LIBs which accounts for approximately 10 wt% of a cell's weight (based on a foil with a ~9 mg cm^{-2} in areal density and ~10 μm in thickness) [19]. The use of thinner and lighter weight of Cu foil collector can directly increase the energy and volume density of LIBs. Conventional methods to fabricate commercial LIB Cu foils are mainly rolling-annealing (RA) and electrodeposition (ED) process [20]. However, both methods come at the challenges regarding the issues of the cost, strength and quality control. RA-Cu foil (Fig. 1) is made by annealing the Cu ingots and then rolled to thin, flat Cu sheets. The disadvantages of the RA Cu foils are the available thickness limited to 6 μm associated with the increased cost of fabrication process. The ED Cu foils (Fig. 1) are fabricated by electroplating the Cu onto a rotating drum from electrolytic solution. The cost of ED foils is lower than RA foils, but the mechanical strength is weaker than RA foils. In addition, prior to usage, both the surfaces of ED- and RA-foils need further treatments to obtain chemically passivated rough surfaces for enhanced slurry adhesion and oxidation prevention [20].

Recently, nanostructure-based current collectors have been reported, including metal foam [21–23], metal array [24,25], graphene sheet [26,27], CNT network [28–30] and Cu based nanomaterials (nanoparticles [31], nanorods [32,33], and nanowires (CuNWs) [34–38]). Nanostructured current collectors can enhance the adhesion of active materials and the penetrability of electrolyte, and release the strain arisen from the volume change during the lithiation/delithiation process [24,36]. However, much of uncertainty about their applicability for practical uses have been raised by the following points: (1) the resistivity of nanostructure current collector is too high [26]; (2) the complicated manufacturing process increases the scale-up difficulty of products; (3) the weight loading in active materials is very low due to incompatibility to conventional slurry-deposited process, resulting in small amount of energy stored in electrodes for practical applications; (4) most electrodes with nanostructures-based current collectors have low practical volume capacity due to their porous structures and low volume density.

Herein, ultra-thin, flexible, light-weight and area-scalable CuNWs foils are fabricated as current collectors for LIBs. The thickness-tunable and density-uniform CuNW foils were made by rolling press drop-casted CuNW fabric (Fig. 1). The anodes made by depositing graphite slurry on CuNW foil current collector (graphite-CuNW foil anode) were assembled to half and full cells to examine the electrochemical performances. The graphite-CuNW foil anode exhibits excellent electrochemical performance during the charge/discharge cycling, even at high loading amount in graphite. The full cell with an areal capacity of 3 mAh g^{-1} remains 80% of the capacity retention over a 600 cycles-period. Moreover, CuNW foils are area-scalable via the foil-making technology. Large-area CuNW foils could be implemented into pouch type full batteries to offer large output capacity. We demonstrate batteries using graphite-CuNW foil anodes can output current > 100 mA h to provide sufficient electricity to power various electronic devices requiring various working conditions, such as light up LED arrays, charge smart phones, power cordless screwdrivers and drone to demonstrate the multiusability in different requirements.

2. Experimental section

2.1. Materials

Copper chloride (CuCl, 99.9%) and oleylamine (70%) were purchased from Sigma–Aldrich. Hexane (ACS) was purchased from Marcon. Graphite powder was purchased from Long Time Technology. Lithium Hexafluorophosphate ($LiPF_6$), electrolyte (1 M $LiPF_6$ in ethylene carbonate (EC): dimethyl carbonate (DMC) 1:1) (v/v), *N*-methyl-2-ptrrolidone (NMP), poly(vinylidone difluoride) (PVDF), super p carbon black, copper metal foil, lithium metal foil, celgard membrane, coin-type cell CR2032 and laminated aluminum film were purchased from Shining Energy. Commercial $Li(NiCoMn)O_2$ cathode electrodes was purchased from Vista Advance Technology. All the chemicals were used without further purification.

2.2. Synthesis of oleylamine-coated copper nanowires

CuCl (1.2 g) and OLA (100 ml) were added to a 100 ml three-neck flask in glovebox. After connected to schlenk line, the solution in flask was stirred magnetically and purged with argon. Until whole of CuCl powder was dissolved, the solution was heated to 110 °C to remove the residual oxygen and water. The color of solution changed from green to yellow after 60 min of heating, and then the temperature was risen to 260 °C and held for 120 min. During this process, the color of solution slowly changed from yellow to reddish. Afterward, the reaction system was cooled to room temperature by water quenching. The reaction mixture was dispersed in hexane and centrifuged at 8000 rpm 5 min for several times until the suspension become clear, and the CuNWs precipitate was collected and dried. The CuNWs after purification were stored in a vial under argon conditions to prevent oxidation.

2.3. Fabrication of CuNW fabric and CuNW foil

The CuNW fabric was prepared by drop casting method.

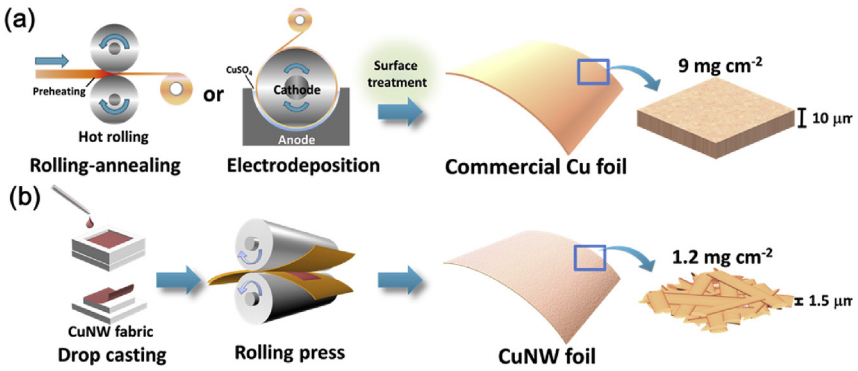

Fig. 1. Schematic of the process of (a) conventional Cu foil fabrication process using rolling-annealing or electrodeposition methods and (b) CuNW foil fabrication process using a rolling press method.

Different amounts of CuNWs were dispersed in hexane in concentration of 10 mg/ml, the CuNW dispersions were dropped into different sizes of square Teflon molds (2 cm × 2 cm and 5 cm × 12 cm). After whole of the hexane was evaporated, the CuNW fabrics were peeled from Teflon molds. Afterward, the CuNW fabrics were annealed in a furnace at 360 °C for 2 h under an atmosphere of 25% hydrogen and 75% argon at a reducing pressure to remove the OLA and reduce the copper oxide to pure copper on the surface of the CuNWs. After annealing, the CuNW fabric were clipped by two pieces of copper foils as substrates and rolled through a roller press machine. The substrates were used to distribute the rolling force onto CuNW fabrics to make uniform CuNW foils. After peeled from copper foils, the thin CuNW foil with metallic luster was obtained. To prevent oxidation, the CuNW foils were stored in argon atmosphere for further uses and characterization.

2.4. Fabrication of electrodes with CuNW foil and Cu foil current collectors

The slurry of electrode was prepared by mixing graphite, super p carbon black and PVDF at a weight ratio of 8:1:1 in NMP as the solvent to form. The slurry was coated on the CuNW foil and copper foil current collectors with different mass loading (6–17 mg cm^{-2} of active material). Next, the electrodes were dried at 80 °C for 2 h follow by an oven baking at 150 °C for 2hr under argon atmosphere to remove whole of solvent.

2.5. Characterization

SEM images were obtained with HITACHI-S4700 scanning electron microscopes. The SEM samples of CuNWs were prepared by dropping the CuNWs in hexane solution onto silicon wafers and drying the solvent. The SEM samples of CuNW foil, copper foil and graphite electrodes with CuNW foil and copper foil current collectors were prepared by adhered the materials onto silicon wafers by carbon tape. TEM image was obtained with HITACHI H-7100 transmission electron microscope. HR-TEM images and diffraction pattern were obtained with a JEOL JEM-3000F electron microscope. The TEM and HR-TEM samples of CuNWs were prepared by dropping the CuNWs in hexane solution onto carbon-coated copper grids and drying. XRD patterns were obtained on a MAC Science MXP18 diffractometer with CuKa radiation. Interfacial shear stress tests of the graphite electrodes with CuNW foil and Cu foil current collector were using SHIMADZU AGS-2000G universal testing machine at a strain rate of 0.5 mm min^{-1}, the samples were cut into 7 mm × 7 mm squares, loaded with ~9 mg of slurry and connected to both sides of grip by 2 pieces of 3M tape.

2.6. LIB assembly and electrochemical characterization

The coin type half cells (CR2032) were assembled in a glovebox which offered an inert atmosphere. Different mass loading of electrodes by using CuNW foil and Cu foil as current collectors were cut into 1 cm × 1 cm of squares as the working electrodes and lithium sheets as the reference electrodes. The electrolyte was 1 M $LiPF_6$ in EC/DMC (1:1 vol%) solution and celgard membrane was used as separator. After aged in room temperature for 30 min, the charge/discharge cyclic performance of graphite electrodes with CuNW foil and copper foil as current collectors was test between 0.01 V and 1.5 V by using Maccor Series 4000. For coin type full cell, the graphite electrodes with CuNW foil current collectors were used as anodes, and commercial $Li(NiCoMn)O_2$ electrodes were used as cathodes. The charge/discharge cyclic performance was test between 2.8 V and 4.2 V by using Maccor Series 4000. For pouch type battery assembly, the large-area (5 cm × 12 cm) graphite anode with CuNW foil current collector was cut into a 4.7 cm × 10 cm rectangle, a nickel tab was connected to the anode, and commercial $Li(NiCoMn)O_2$ cathode connected to an aluminum tab. Next, the anode, separator and cathode were fixed on an aluminum laminated film. After injecting the electrolyte, the aluminum laminated film was sealed by a compact heating sealer in glovebox. Charging/discharging cyclic performance of pouch type battery was test between 2.8 V and 4.2 V by using Maccor Series 4000.

3. Results and discussion

CuNWs with diameters of 70–120 nm and lengths longer than 30 μm were synthesized by via a self-seed growth in organic solution [39–41]. The five-fold twinned CuNWs were synthesized by using a heating-up method and seed-mediated growing mechanism in organic solution. Oleylamine (OLA) was used as solvent, reducing agent and soft template in the reaction. After all of CuCl precursor was dissolved in OLA and the temperature of solution was increased to 110 °C, a clear yellow Cu^{+}-OLA complex was generated. When the temperature of solution reached 260 °C, Cu atoms were reduced from Cu^{+}-OLA complex. Under this temperature, Cu^{+} ions were disproportionated into metallic Cu^{0} and Cu^{2+} ions. Further, the Cu atoms assembled to become Cu nanoparticles, and the CuNWs were formed by using these Cu nanoparticles as the seed. The details of characterization of CuNWs are showed in Fig. S1 in supporting information.

Fig. 2(a) reveals a large amount of CuNWs arranged randomly and tend to interlace to form a mesh structure [42]. CuNW suspension in hexane at a concentration of 10 mg ml^{-1} was dropped into a 2 cm × 2 cm Teflon mold. After hexane dried, a reddish CuNW films was formed and peeled up to form a freestanding fabric. Fabrics were annealed at 360 °C under Ar/H_2 atmosphere. The intimate contact junctions between CuNWs were created because the partial melting occurred on the adjacent CuNWs which improve the electronic conductivity and mechanical strength of CuNW fabrics [43]. The surface topography of the CuNW fabric composed of randomly arranged NWs is porous and fluffy (Fig. 2(b)). Areal densities of CuNW fabric are determined by the amount of loaded CuNWs into the molds where the fabric thicknesses change proportionally (Fig. 2(c)).

CuNW foils were obtained by pressing the CuNW fabrics using a roller press machine. Unlike solid Cu foil (Fig. S2), the surface morphology of CuNW foil exhibits porous structure and appears brighter surface compared to Cu NW fabric (Fig. 3(a)). Closer imaging of a CuNW foil (Fig. 3(b)) shows a fabric-liked porous structure weaved by squashed CuNWs, and the contact junctions between CuNWs were partially sintered. The internal structure was composed of distorted CuNWs, and lots of tiny channels exist between nanowires, whereas the Cu foil is solid bulk Cu. Porous, fused interconnected structures of CuNW foils provide more surface area for slurry adhesion, and improved electrical conductivity compared to CuNW fabric [44]. The thickness of CuNW foils can be tuned by using fabrics of different areal densities. Fig. 3(c) shows CuNW foils with 12, 28, 32, 40, 55 μm made from areal mass density of 1, 2, 3, 4, 5 mg/cm^2, respectively, which shows linear relationship between areal mass density and thickness (Fig. 3(d)). The average volume density of CuNW foils still has ~8.5 g cm^{-3} (Fig. 3(e)), which is in approximately 96% of bulk Cu (8.9 g cm^{-3}). Different from fluffy structure of nanomaterial current collectors with low volume density (~1 g cm^{-3}), the compact structure of CuNW foil has ability to improve the mechanical strength and reduce the volume occupied in a battery, in other words, the volume capacity of an electrode can be increased. We can make CuNW foil with a thickness as

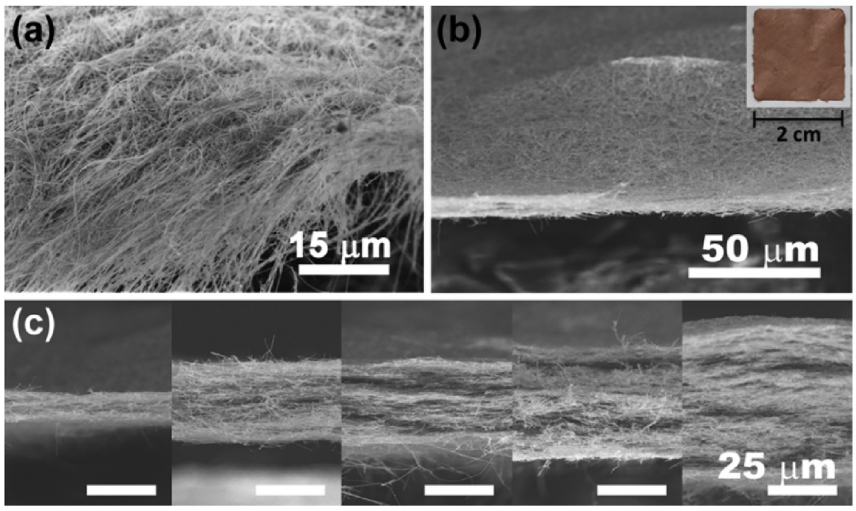

Fig. 2. (a) SEM image of numerous of tangled CuNWs. (b) Photograph and SEM image of the CuNW fabric (c) cross-sectional SEM images of CuNW fabrics with different weight loading (~1, 2, 3, 4 and 5 mg cm^{-2} from left to right).

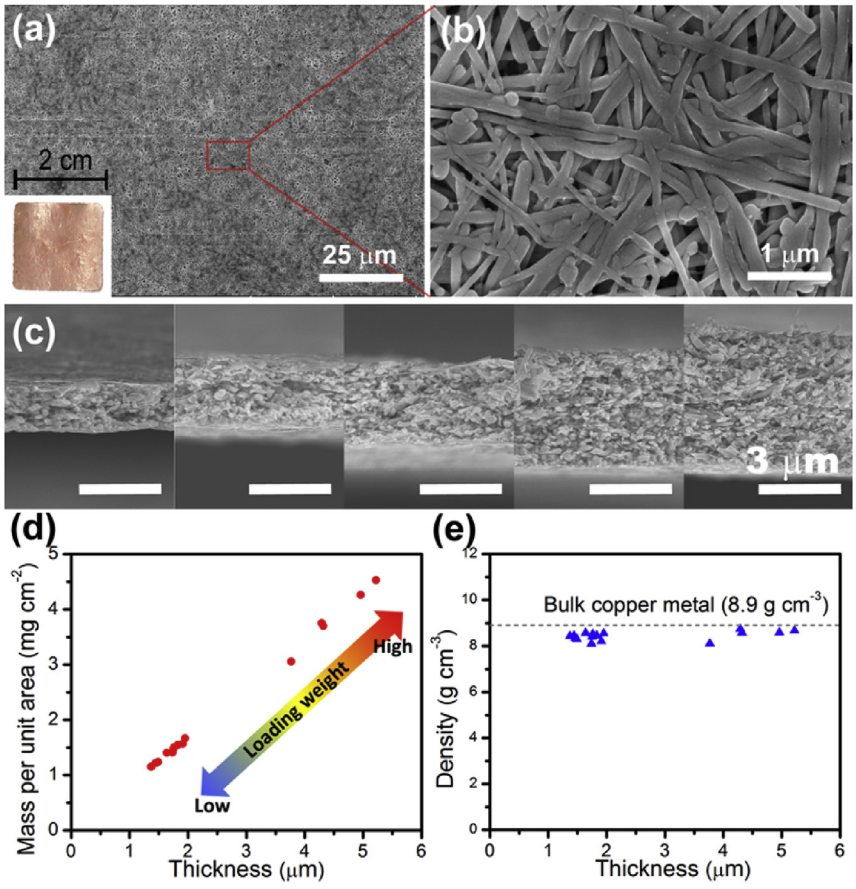

Fig. 3. (a) The photographs and top view SEM images of CuNW foil. (b) The top view SEM images of CuNW foil in higher resolution. (c) The cross sectional SEM images of CuNW foil with different weight loading (~1, 2, 3, 4 and 5 mg cm^{-2} from left to right). (d) Thickness (μm) vs mass per unit area (mg/cm^2) and (e) Thickness (μm) vs volume density (g/cm^3) of CuNW foils made from different materials loading.

low as ~1.5 μm, which is 6.7 times thinner than the commercial Cu foil (~10 μm). The areal density of 1.5 μm thick CuNW foil is ~1.2 mg cm^{-2}, only two-fifteenths of commercial Cu foil (~9 mg cm^{-2}). The sheet resistance of the 1.5 μm thickness of CuNW foil was measured to be ~24 mΩ sq^{-1}, very close to commercial Cu foil (~10 mΩ sq^{-1}), but substantially lower than other nanomaterial-based current collector such as CNT (66Ω sq^{-1}) [28] and graphene (0.8Ω sq^{-1}) [26]. In addition, the EIS measurements of graphite-based half-cell with CuNW foil and commercial Cu foil current collector indicate high electrochemical similarity (Fig. S4 in

revised supporting information). The cost of fabricating process of CuNW foils can be reduced due to the facile and reusable equipment. Comparing to RA and ED foil, CuNW foil only requires a place for CuNWs depositing. Moreover, once-rolling and solvent-recyclable process of CuNW foils has ability to decrease the materials waste and energy consumption.

1.5 μm thick CuNW foil is used as a current collector for LIBs using graphite as an active material. The slurry with a solid mass fraction of 80 wt% of graphite was coated on CuNW foils. Fig. 4(a) shows the cross sectional SEM image of a graphite-CuNW foil electrode with a 67 μm graphite layer coated on the CuNW foil. The graphite-CuNW foil electrode is flexible and the graphite layer exhibits strong adhesion (Fig. 4(b)). The graphite-CuNW foil electrodes were cut into 1 cm × 1 cm to be applied in electrochemical testing. The both sides of graphite-CuNW foil electrode were shown in Fig. 4(c). The CuNW foil side shows binder penetrated the current collector through the pores on the surface and the channels in the internal of CuNW foil (Fig. 4(d)), showing the binder not only adheres on the surface but also adhere inside the internal region of current collector. The wetting properties at the interfaces of graphite-CuNW foil and graphite-Cu foil were examined by measuring the contact angles between slurry/current collector interfaces. Two 20 μl droplets of slurry were dropped on CuNW foil and Cu foil, respectively. As Fig. 4(e) and (g) reveal, the contact angle at graphite-CuNW foil is measured to be 32°, which is smaller than graphite-Cu foil (46°). This is resulted from the smaller surface tension at the graphite-CuNW foil interface [28]. In addition, when slurry solution was dropped onto the CuNW foil, binder solution appears to spread out from the central location via capillary force as shown in Fig. 4(f), whereas solution stay still on Cu foil (Fig. 4(h)). This result shows binder solution adheres better to Cu NW foil than to Cu foil [45,46].

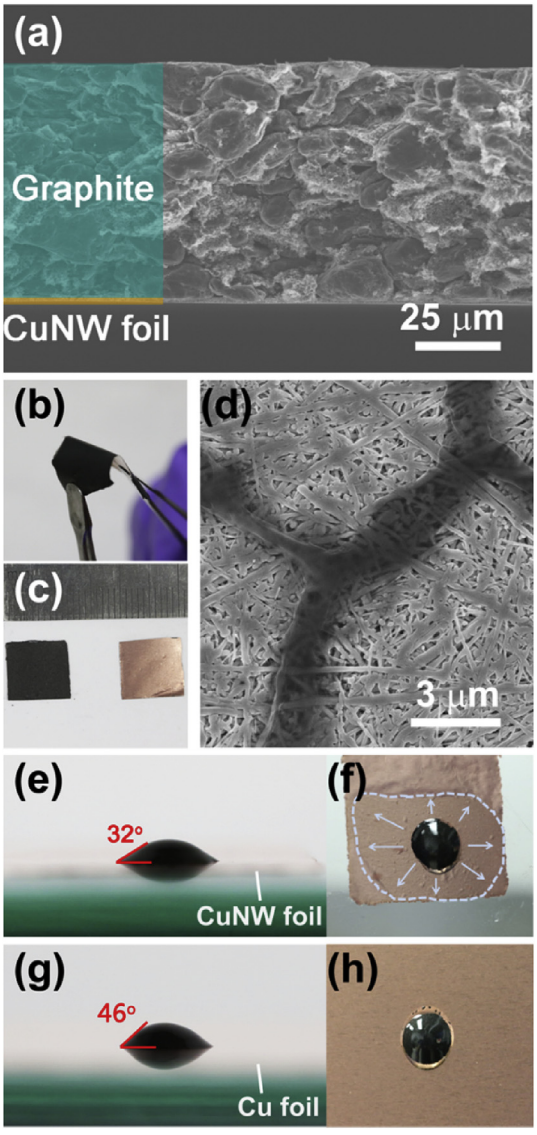

Fig. 4. (a) Cross sectional SEM image of graphite-CuNW foil anodes. (b) Photograph of a curved 2 cm × 2 cm graphite-CuNW foil electrode material. (c) Both sides of 1 cm × 1 cm graphite-CuNW foil electrode. (d) SEM image of the current collector side of electrode. (e,g) Photographs of the graphite slurry droplet on the CuNW foil and Cu foil, the contact angle of both droplets were measured. (f,h) The comparison of top-view photographs of graphite slurry droplet on the CuNW foil and Cu foil.

The characterization of interface adhesion of graphite-CuNW and graphite-Cu foil electrodes was determined by single-lap shear tests (Fig. 5(a)) [47] The shear strength of graphite-CuNW foil electrode was measured to be ~0.067 MPa, which is nearly 2.8 times interfacial adhesion performance higher than the graphite-Cu foil electrode (~0.024 MPa). After testing, the slurry and the current collectors were separated by tapes, as Fig. 5(b) shows, most of slurry was removed from Cu foil and there are hardly any graphite left on the Cu foil. In contrast, some graphite still left on the CuNW foil. This result offers the direct evidence that interfacial adhesion at the graphite/CuNW foil interface is stronger than the graphite/Cu foil interface, resulting in good toleration for volumetric change and mechanical strain during repeated cycling, even at large current.

The cycling performance of graphite-CuNW foil electrodes in a half cell at 0.1C (6 mg of graphite loading, ~0.23 mA of current) was shown in Fig. 6(a). In order to make stable growth of solid-electrolyte interface (SEI) film, the 0.05C of charge-discharge rate

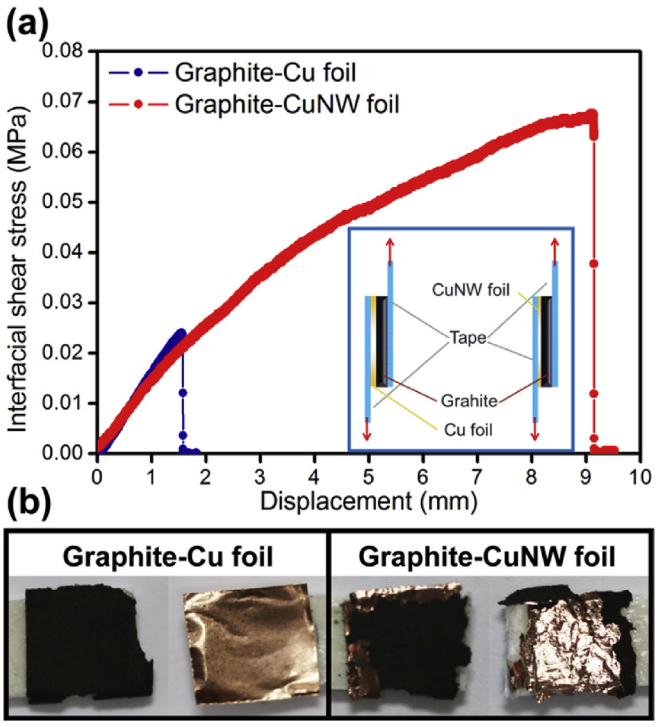

Fig. 5. (a) The results of interfacial shear tests of the graphite-CuNW foil and graphite-Cu foil electrodes. Inset: scheme of the experimental setup. (b) Photographs of the graphite-CuNW foil and graphite-Cu foil electrodes after testing.

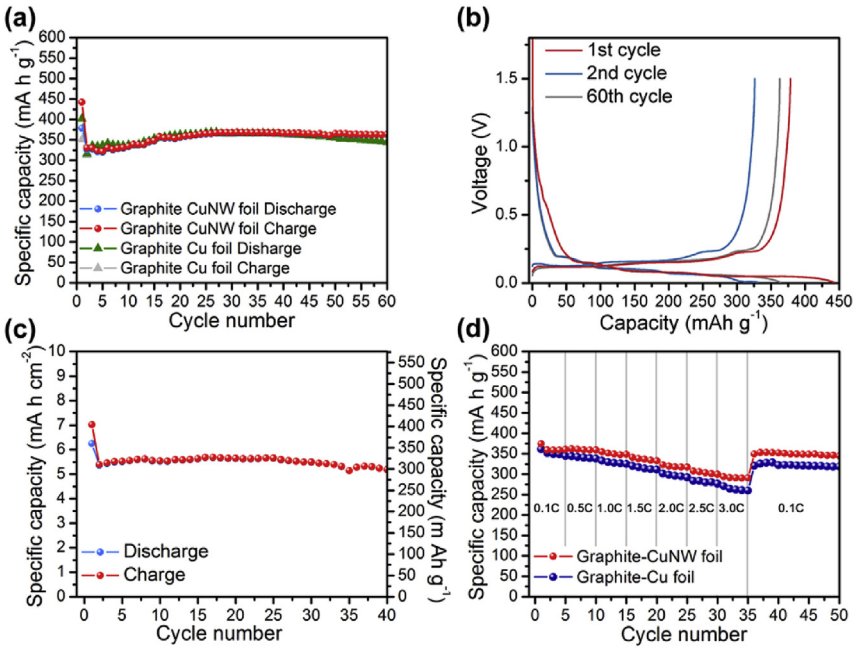

Fig. 6. (a) Cycling performance of graphite-CuNW foil and graphite-Cu foil anodes with EC/DMC electrolyte at a rate of 0.1 C. (b) Cyclic voltammograms of graphite-CuNW foil anode at 0.1 C of charge-discharge cycling test. (c) Cycling performance of high loading graphite-CuNW foil anode at a rate of 0.1 C. (d) Discharging performance of graphite-CuNW foil and graphite-Cu foil anodes at various rates of 0.05 C, 0.1 C, 0.5 C, 1.0 C, 1.5 C, 2.0 C, 2.5 C and 3.0 C for total 50 cycles.

was set at first cycle. In Fig. 6(a), the graphite-CuNW foil electrode exhibits outstanding specific discharge capacity of 363 mA h g^{-1} and good cycling stability after 60 cycles, which was similar to performance of the graphite-Cu foil electrode. Fig. 6(b) shows the cyclic voltammograms of the graphite-CuNW foil electrode from the 0.1C cycling test. In the first charge curve, a plateau appeared at ~0.5 V corresponds to the SEI formation on the surface of electrode [48]; the plateau appeared at ~0.2 V corresponds to the formation of LiC_6 [49]. At all discharge curves, a long plateau appeared at ~0.4 V suggests the lithium de-intercalation from graphite [49]. The specific charging capacity at the first cycle (441.8 mA h g^{-1}) is higher than the theoretical capacity of graphite (372 mA h g^{-1}) due to larger area of the contact between graphite and electrolyte resulted from the porous current collector, leading to more formation of SEI and other side reactions [50,51]. Fig. 6(c) shows the cyclic performance graphite-CuNW foil electrode at a high loading in graphite. The electrode loaded in graphite areal weight of 17 mg cm^{-2} corresponds to an areal capacity of 5 mA h cm^{-2}. The

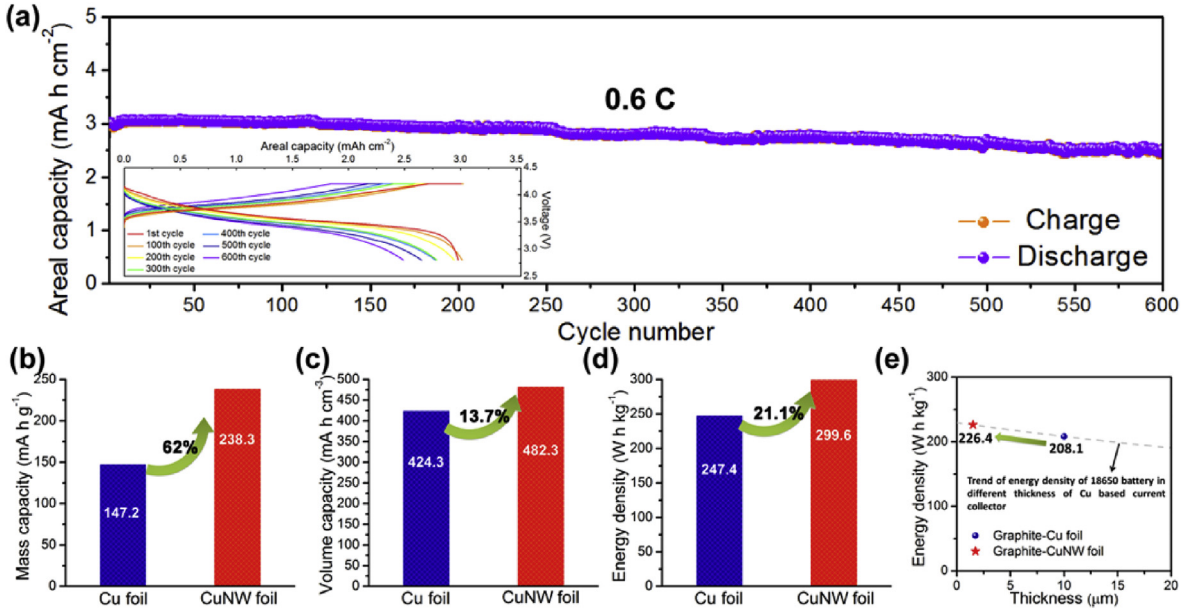

Fig. 7. (a) Long-term cycling performance and cyclic voltammograms of graphite-CuNW foil anode in a full cell at a rate of 0.6 C. The comparison of commercial graphite-Cu foil anode and graphite-CuNW foil anode with (b) mass specific capacity, (c) volume specific capacity and (d) energy density comparison at whole electrodes level. (e) Plot of energy density vs Cu foil thickness for a 18650 type LIB.

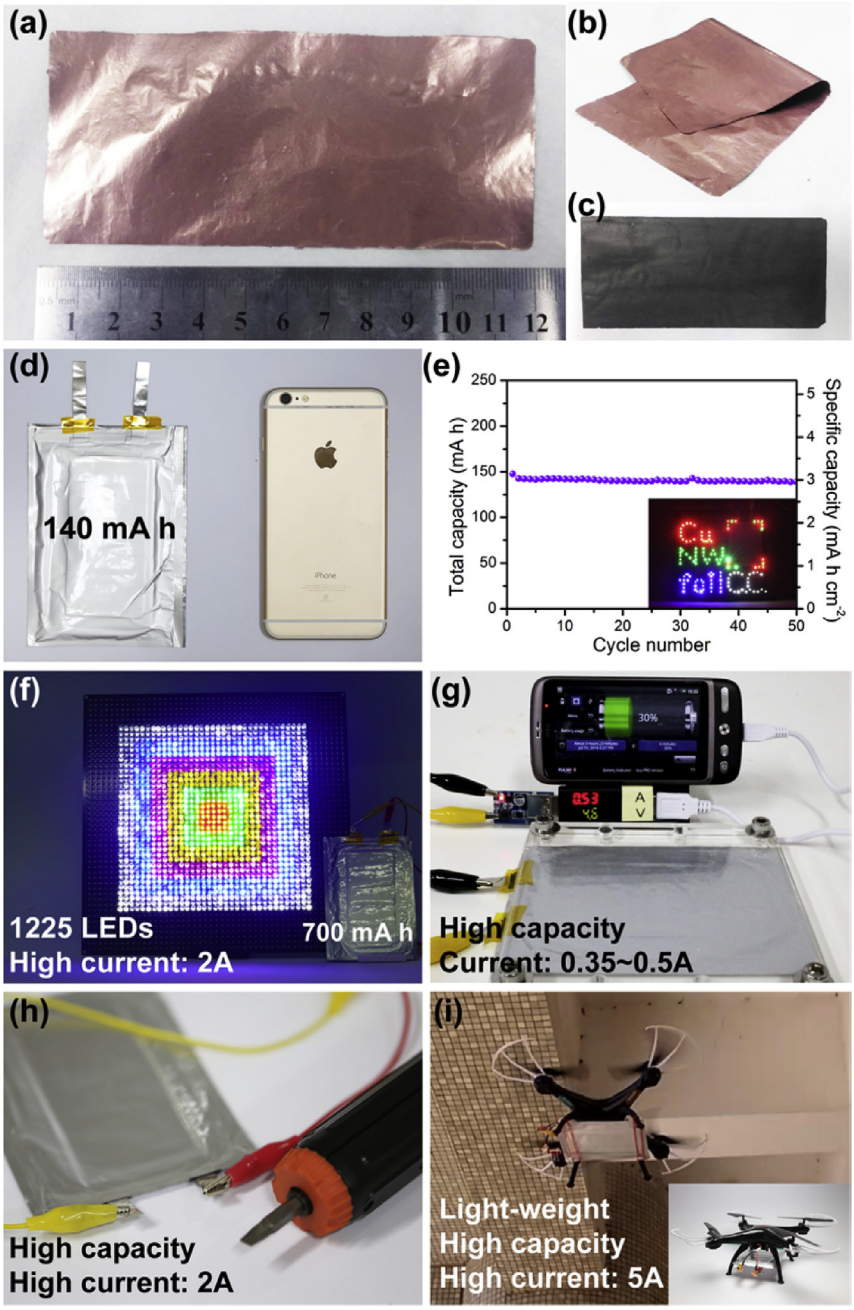

Fig. 8. Photographs of (a) a 5 cm × 12 cm CuNW foil, (b) the CuNW foil folded, (c) the graphite-CuNW foil electrode, (d) a 4.7 cm × 10 cm pouch type full cell. (e) Cycling performance of the pouch type full cell (d) at a rate of 0.6 C. A 700 mAh pouch battery comprising five pieces of 4.7 cm × 10 cm graphite-CuNW foil was demonstrated to (f) light up over 1225 LEDs with different color, (g) charge the smart phone, (h) power the cordless screwdriver, and (i) fly the drone. (For interpretation of the references to colour in this figure legend, the reader is referred to the web version of this article.)

5 mAh cm^{-2} graphite-CuNW foil electrode remains 300 mA h g^{-1} of specific discharge capacity at 0.1 C after 40 cycles, indicating high loading endurance of CuNW foil current collector. Fig. 6(d) shows the discharge performance of graphite-CuNW foil electrode at different rates (0.05C at first cycle, 0.1C at 2 to 5 cycle, afterward, 0.5 C, 1.0 C, 1.5 C, 2.0 C, 2.5 C and 3.0 C were examined successively). In the charging step, the half-cell was charged at constant current initially, and then change to trickle charging until to the end of the step. The discharge capacity of graphite-CuNW foil electrode were 360.4 mA h g^{-1} (0.1C), 359.2 mA h g^{-1} (0.5C), 348.9 mA h g^{-1} (1.0C), 332.6 mA h g^{-1} (1.5 C), 317.2 mA h g^{-1} (2.0C), 300 mA h g^{-1} (2.5C), and 290.9 mA h g^{-1} (3.0C). All of the discharge capacities of graphite-CuNW foil are higher than the values of graphite-CuNW foil electrode. After discharging at 3C, the charge-discharge rate was reinstated to 0.1C and continued the testing to 50 cycles. At 50^{th} cycle, discharge capacity maintains 345 mA h g^{-1}.

The coin-type full cells using a graphite-CuNW foil anode and a Li(NiCoMn)O_2-Al foil cathode were fabricated. The cell has an areal specific capacity of around 3 mA h cm^{-2} [52]. In order to prevent dendrite formation, the total capacities loaded on anode was 10% more than the total capacities on the cathode. Fig. 7(a) shows the cyclic voltammograms of the cell at 0.1C between 2.8 V and 4.2 V. At the charging stage, the voltage rose slowly from 3.6 V to 4.2 V followed by a short constant-voltage charging process. At the

discharging process, there is a broad plateau at 4.2 V and terminates at 3.5 V, corresponding to the stable and high working voltage. To estimate the commercial feasibility, the full cell was examined by a 600-cycles period at 0.6C to simulate usage conditions of LIBs in handheld devices. Fig. 7(a) shows the cycling performance of full cell after 2 cycles of stabilizing process. The cell's areal specific capacity is ~3 mA h cm^{-2} during the initial 120 cycles at a 0.6C of charge-discharge rate. After 600 cycles, it still has 83.6% capacity retention, showing the excellent cycling stability at 3.7 V of the working voltage, which reaches the standard of iPhone batteries, i.e., 80% capacity retention after 500 cycles of complete charge. The average coulombic efficiency for cycles from the 1st to 600th is 99.76%, very close to 100%. CuNW foil-based LIBs have several characteristics to rival the commercial rechargeable Cu foil-based LIBs. The mass and volume specific capacity of the whole anode can be significantly improved by the replacement of Cu foil by CuNW foil. The mass specific capacity of a graphite-CuNW foil anode is 238.3 mA h g^{-1}, which is 62% higher than a graphite-Cu foil anode (147.2 mA h g^{-1}); the volume specific capacity is 482.3 mA h cm^{-3} for CuNW foil, which is 13.7% higher than that of commercial Cu foil (424.3 mA h cm^{-3}) (Fig. 7(b) and (c)). In addition, we assume an optimized anode and cathode system that supplies 3 mA h cm^{-2} of capacity and the working voltage is 3.7 V. Based on these assumptions, the energy density of a full cell using CuNW foil current collector is 21.1% higher than that using Cu foil (Fig. 7(d)). The detail of calculation is described in Table S1 in supporting information. In an 18650 type LIB, more active materials can be loaded to obtain higher energy density due to decreased weight and thickness of anode current collectors. In Fig. 7(e), the energy density of 18650 type battery with CuNW foil is 226.4 W h kg^{-1}, approximately of 98.7% to the maximum energy density of 229.5 W h kg^{-1}, i.e., the thickness of current collector is assumed to be 0. The details of calculation are described in Tables S2 and S3 in supporting information.

The overall manufacturing process of Cu NW foils can be easily area-scalable by using large deposition molds. Fig. 8(a) shows a 5 cm × 12 cm CuNW foil fabricated from mold with the same size. The 5 cm × 12 cm CuNW foil is flexible and can be directly coated with graphite slurry to make graphite-Cu NW foil electrode Fig. 8(b–c). The graphite-Cu NW foil electrode was implemented into a 4.7 cm × 10 cm pouch cell. The battery fabrication process was shown in Fig. S6. (Fig. 8(d) shows a pouch type full cell which can supply ~140 mA h of capacity with a cell size suitable to be implemented into iPhone 6 plus. The discharging capacity of the pouch battery at a rate of 0.6 C (the rate at first cycle is 0.05C) is almost no decay (Fig. 8(e)) and the areal capacity of the pouch battery remained ~3 mA h cm^{-2} after 50 cycles. The 140 mAh cell was applied to light up more than 120 LEDs composed of different colors. We also assembled five pieces of 4.7 cm × 10 cm graphite-CuNW foil into a laminated pouch battery to offer ~700 mA h output capacity. As Fig. 8(f) shows, 1225 LEDs with a current of 2 A with different colors and driving voltages from 3 V to 3.5 V were lighted up successfully. The 700 mA h pouch battery was applied to charge the smart phone where the charging current and voltage were tuned to 0.5 A and 4.5 V through a power booster (Fig. 8(g) and Video S1). The pouch battery was also examined to apply on cordless screwdrivers which require high current (2 A) and capacity output devices (Fig. 8(h)). Video S2 shows the cordless screwdriver is powered to fasten a screw into a cabinet. Finally, the battery can also power the drone needs combination of the requirements of discharging rate of 5 A, high capacity, and light weight (Fig. 8(i) and Video S3).

Supplementary video related to this article can be found at http://dx.doi.org/10.1016/j.jpowsour.2017.02.041.

4. Conclusion

In summary, Cu NW foils have been demonstrated as ultrathin and light-weight anode current collectors for LIBs. The following advantages show how CuNW foil can advance the LIB battery technology: (1) lighter, thinner and higher energy density of LIBs can be achieved with Cu NW foil implemented into the battery components. (2) The rough surface and porous internal structure of CuNW foils not only enable good wetting and adhesion of active material slurry but also perform high cycling stability in high-loading active materials. These characteristics are important to accommodate the dramatic volume change of high-capacity active materials such as Si, Ge and P during charge/discharge process. (3) CuNW foils are highly conductive and exhibit current durability, leading to low over-potential of LIBs for electric vehicle batteries (EVBs) applications. (4) Realizable large-area and continuous production of CuNW foils provides a fast and reliable supply chain to satisfy the huge demand of lithium-ion battery industry. Therefore, we envision CuNW foil may become an alternative replacement to traditional Cu foil as anode current collector in LIBs, or other applications such as printed circuit board (PCB).

Acknowledgments

We acknowledge the financial support by the Ministry of Science and Technology of Taiwan through the grants of NSC 102-2221-E-007-023-MY3, MOST 103-2221-E-007-089-MY3, MOST 103-2622-E-007-025, and MOST 102 – 2633-M-007-002.

Appendix A. Supplementary data

Supplementary data related to this article can be found at http://dx.doi.org/10.1016/j.jpowsour.2017.02.041.

References

[1] S. Choi, J. Kim, M. Eom, X. Meng, D. Shin, J. Power Sources 299 (2015) 70–75.
[2] Z. Lu, N. Liu, H.-W. Lee, J. Zhao, W. Li, Y. Li, Y. Cui, ACS Nano 9 (3) (2015) 2540–2547.
[3] C. He, S. Wu, N. Zhao, C. Shi, E. Liu, J. Li, ACS Nano 7 (5) (2013) 4459–4469.
[4] Y. Liu, J. Guo, J. Zhang, Q. Su, G. Du, Appl. Surf. Sci. 324 (2015) 399–404.
[5] S. Pacala, R. Socolow, Science 305 (5686) (2004) 968–972.
[6] M.M. Thackeray, C. Wolverton, E.D. Isaacs, Energy Environ. Sci. 5 (7) (2012) 7854–7863.
[7] M. Armand, J.M. Tarascon, Nature 451 (7179) (2008) 652–657.
[8] M.T. McDowell, S.W. Lee, I. Ryu, H. Wu, W.D. Nix, J.W. Choi, Y. Cui, Nano Lett. 11 (9) (2011) 4018–4025.
[9] J.M. Tarascon, M. Armand, Nature 414 (6861) (2001) 359–367.
[10] N. Nitta, F. Wu, J.T. Lee, G. Yushin, Mater. Today 18 (5) (2015) 252–264.
[11] S. Xin, Y.-G. Guo, L.-J. Wan, Acc. Chem. Res. 45 (10) (2012) 1759–1769.
[12] C.K. Chan, H. Peng, G. Liu, K. McIlwrath, X.F. Zhang, R.A. Huggins, Y. Cui, Nat. Nanotechnol. 3 (1) (2008) 31–35.
[13] I.H. Son, J. Hwan Park, S. Kwon, S. Park, M.H. Rummeli, A. Bachmatiuk, H.J. Song, J. Ku, J.W. Choi, J.-M. Choi, S.-G. Doo, H. Chang, Nat. Commun. (2015) 6.
[14] E. Peled, F. Patolsky, D. Golodnitsky, K. Freedman, G. Davidi, D. Schneier, Nano Lett. 15 (6) (2015) 3907–3916.
[15] F.-W. Yuan, H.-Y. Tuan, Chem. Mater. 26 (6) (2014) 2172–2179.
[16] A.S. Arico, P. Bruce, B. Scrosati, J.-M. Tarascon, W. van Schalkwijk, Nat. Mater. 4 (5) (2005) 366–377.
[17] X. Li, Z. Yang, Y. Fu, L. Qiao, D. Li, H. Yue, D. He, ACS Nano 9 (2) (2015) 1858–1867.
[18] T. Kennedy, E. Mullane, H. Geaney, M. Osiak, C. O'Dwyer, K.M. Ryan, Nano Lett. 14 (2) (2014) 716–723.
[19] L.-F. Cui, L. Hu, J.W. Choi, Y. Cui, ACS Nano 4 (7) (2010) 3671–3678.
[20] D. Lu, C.P. Wong, Materials for Advanced Packaging, Springer, 2008, p. 724.
[21] B. Qu, L. Hu, Q. Li, Y. Wang, L. Chen, T. Wang, ACS Appl. Mater. Interfaces 6 (1) (2014) 731–736.
[22] C. Zhao, S. Li, X. Luo, B. Li, W. Pan, H. Wu, J. Mater. Chem. A 3 (18) (2015) 10114–10118.
[23] J. Wang, Q. Zhang, X. Li, D. Xu, Z. Wang, H. Guo, K. Zhang, Nano Energy 6 (2014) 19–26.
[24] S.R. Gowda, A. Leela Mohana Reddy, X. Zhan, H.R. Jafry, P.M. Ajayan, Nano Lett. 12 (3) (2012) 1198–1202.

[25] S. Zhang, Z. Du, R. Lin, T. Jiang, G. Liu, X. Wu, D. Weng, Adv. Mater. 22 (47) (2010) 5378–5382.
[26] Y. Chen, K. Fu, S. Zhu, W. Luo, Y. Wang, Y. Li, E. Hitz, Y. Yao, J. Dai, J. Wan, V.A. Danner, T. Li, L. Hu, Nano Lett. 16 (6) (2016) 3616–3623.
[27] G. Zhou, S. Pei, L. Li, D.-W. Wang, S. Wang, K. Huang, L.-C. Yin, F. Li, H.-M. Cheng, Adv. Mater. 26 (4) (2014) 625–631.
[28] K. Wang, S. Luo, Y. Wu, X. He, F. Zhao, J. Wang, K. Jiang, S. Fan, Adv. Funct. Mater. 23 (7) (2013) 846–853.
[29] S. Yehezkel, M. Auinat, N. Sezin, D. Starosvetsky, Y. Ein-Eli, J. Power Sources 312 (2016) 109–115.
[30] K.-H. Choi, S.-J. Cho, S.-J. Chun, J.T. Yoo, C.K. Lee, W. Kim, Q. Wu, S.-B. Park, D.-H. Choi, S.-Y. Lee, S.-Y. Lee, Nano Lett. 14 (10) (2014) 5677–5686.
[31] L. Liu, B.G. Choi, S.O. Tung, T. Hu, Y. Liu, T. Li, T. Zhao, N.A. Kotov, Faraday Discuss. 181 (0) (2015) 383–401.
[32] P.L. Taberna, S. Mitra, P. Poizot, P. Simon, J.M. Tarascon, Nat. Mater. 5 (7) (2006) 567–573.
[33] G. Kim, S. Jeong, J.-H. Shin, J. Cho, H. Lee, ACS Nano 8 (2) (2014) 1907–1912.
[34] C. Hwang, T.-H. Kim, Y.-G. Cho, J. Kim, H.-K. Song, Sci. Rep. 5 (2015) 8623.
[35] G.-H. Lee, H.-W. Shim, D.-W. Kim, Nano Energy 13 (2015) 218–225.
[36] R. Lin, S. Zhang, Z. Du, H. Fang, Y. Ren, X. Wu, RSC Adv. 5 (106) (2015) 87090–87097.
[37] R. Lin, S. Zhang, Y. Ren, X. Wu, H. Fang, X. Wei, RSC Adv. 6 (24) (2016) 20042–20050.
[38] L.-L. Lu, J. Ge, J.-N. Yang, S.-M. Chen, H.-B. Yao, F. Zhou, S.-H. Yu, Nano Lett. 16 (7) (2016) 4431–4437.
[39] E. Ye, S.-Y. Zhang, S. Liu, M.-Y. Han, Chem. - Eur. J. 17 (11) (2011) 3074–3077.
[40] H.-J. Yang, S.-Y. He, H.-Y. Tuan, Langmuir 30 (2) (2014) 602–610.
[41] H.-C. Chu, Y.-C. Chang, Y. Lin, S.-H. Chang, W.-C. Chang, G.-A. Li, H.-Y. Tuan, ACS Appl. Mater. Interfaces 8 (20) (2016) 13009–13017.
[42] A.M. Chockla, J.T. Harris, V.A. Akhavan, T.D. Bogart, V.C. Holmberg, C. Steinhagen, C.B. Mullins, K.J. Stevenson, B.A. Korgel, J. Am. Chem. Soc. 133 (51) (2011) 20914–20921.
[43] F. Cui, Y. Yu, L. Dou, J. Sun, Q. Yang, C. Schildknecht, K. Schierle-Arndt, P. Yang, Nano Lett. 15 (11) (2015) 7610–7615.
[44] Z. Zheng, Z. Wang, X. Song, S. Xun, V. Battaglia, G. Liu, ChemSusChem 7 (10) (2014) 2853–2858.
[45] L. Miao, L. Lu, T. Fu, Y. Tang, B. Tang, Appl. Phys. A 120 (1) (2015) 255–263.
[46] B. June Zhang, K. Kim, J. Appl. Phys. Lett. 101 (5) (2012) 054104.
[47] W. Su, J.O. Iroh, Synth. Met. 114 (3) (2000) 225–234.
[48] H. Zheng, K. Jiang, T. Abe, Z. Ogumi, Carbon 44 (2) (2006) 203–210.
[49] P. Guo, H. Song, X. Chen, Electrochem. Commun. 11 (6) (2009) 1320–1324.
[50] M.S. Yazici, D. Krassowski, J. Prakash, J. Power Sources 141 (1) (2005) 171–176.
[51] M. Winter, J.O. Besenhard, M.E. Spahr, P. Novák, Adv. Mater. 10 (10) (1998) 725–763.
[52] Y.-K. Sun, M.-J. Lee, C.S. Yoon, J. Hassoun, K. Amine, B. Scrosati, Adv. Mater. 24 (9) (2012) 1192–1196.